A Non-Linear Iterative Method for Multi-Layer DOT Sub-Surface Imaging System

Hsiang-Wen Hou, Shih-Yang Wu, Hao-Jan Sun, and Wai-Chi Fang

***Abstract*—Diffuse Optical Tomography (DOT) has become an emerging non-invasive technology, and has been widely used in clinical diagnosis. Functional near-infrared (FNIR) is one of the important applications of DOT. However, FNIR is used to reconstruct two-dimensional (2D) images for the sake of good spatial and temporal resolution. In this paper we propose a multiple-input and multiple-output (MIMO) based data extraction algorithm method in order to increase the spatial and temporal resolution. The non-linear iterative method is used to reconstruct better resolution images layer by layer. In terms of theory, the simulation results and original images are nearly identical. The proposed reconstruction method performs good spatial resolution, and has a depth resolutions capacity of three layers.**

Keywords—Reconstruction Algorithm; Iterative Method; Three Dimensional; Diffuse Optical Tomography; Spatial Resolution; Monte Carlo;

I. INTRODUCTION

In recent years, Diffuse Optical Tomography (DOT) has represented a fast growing technology, and has currently been developed into a mature technology. DOT is a low-cost and sensitive approach to reconstruct the image of a high scattering medium such as tissue. Due to the weak absorption at the near-infrared wavelengths of oxygenated hemoglobin (HbO) and deoxygenated hemoglobin (Hb) [2] [3], DOT uses near-infrared spectroscopy (NIRS) to monitor the local changes of the HbO and Hb concentration variations. By using the Modified Beer-Lambert Law (MBLL), changes in absorption values in the spectrum of NIRS permits us to find out concentration variations of Hb and HbO. The NIRS produces results by analyzing the data measured from the source-detector pair. The spatial resolution is decided via distance and the number of source-detector pairs. Detectors can improve the spatial resolution by receiving alternatively optical intensity from different sources. One disadvantage of NIRS is that it is not easy to detect depth information because photons might be absorbed by tissue on their diffusion path, so we should have another method to overcome this problem.

The proposed approach helps us to reconstruct the desired image by combining information from different source-detector pairs. This algorithm is based on a hexagonal source and detector array structure with three layers of depth. One of the advantages of this algorithm is to increase the spatial resolution so we can apply a non-linear iterative approach to make convergence easier. Another advantage is that this algorithm can reconstruct three layers, which is its main difference with conventional reconstruction.

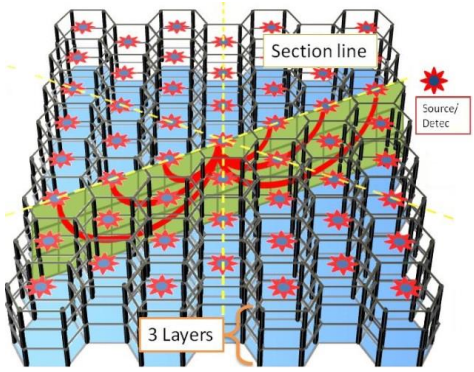

Figure 1. The 3D hexagonal Source-Detector array structure

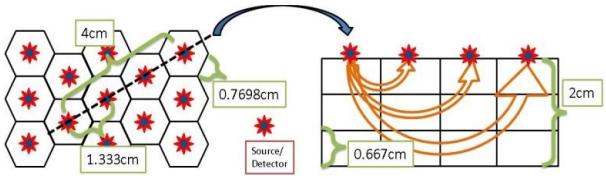

Figure 2. The top view

Figure 3. The side view

II. THE ALGORITHM CONCEPT

Fig. 1 is a perspective view that shows the hexagonal Source-Detector (SD) array structure with three layers. The symbol in the center of each hexagon represents two parts, one is the source and the other is the detector. The source and detector at the same location are not excited simultaneously. Fig. 2 is the top view of SD array, and this array is symmetrical with respect to the yellow-dashed lines. Fig. 3 is the cross section view of the hexagonal structure, it shows that different distances between sources/detectors cause different diffusion depth. This research uses the non-linear iterative method which is a mathematical procedure to improve approximate solutions. An iterative method uses repeated calculations to make the error lower than the given initial value and increase the accuracy of the experimental results.

This work was supported in part by the National Science Council of Taiwan, R.O.C.

Hsiang-Wen Hou is with Department of Electronics Engineering, National Chiao Tung University, 1001 University Road, Hsinchu, Taiwan (R.O.C.)(shyan790804@gmail.com).

Shih-Yang Wu is with Department of Electronics Engineering, National Chiao Tung University, 1001 University Road, Hsinchu, Taiwan (R.O.C.)(nasam13@hotmail.com).

Hao-Jan Sun is with Institute of Biomedical Engineering, National Chiao Tung University, 1001 University Road, Hsinchu, Taiwan (R.O.C.)(t085721@gmail.com).

Wai-Chi Fang is with Department of Electronics Engineering, National Chiao Tung University, 1001 University Road, Hsinchu, Taiwan (R.O.C.)(wfang@mail.nctu.edu.tw).

A. Photons propagation

When photons propagate from the light source to the light detector, the optical density can be received by the detector. It can be described by the modified Beer-Lambert Law:

$$I_d = I_i \times \sum_m \{R_m \times \prod_n [\exp(-\epsilon C_n U P_n)]\} \times \exp(-g) \quad (1)$$

I_d is the optical intensity which is received by the detector after propagation. I_i is the intensity of the incident light. R_m is the possibility of the light source and the receiver with diffusing paths of different depth. ϵ is the extinction coefficient of the molecules (cm-1mM-1). C_n is the concentration of the molecules (mM). U is the size of each reconstructed grid which is defined as 0.667 (cm) in this system. P_n is a differential path length factor (DPF), which is the ratio of real length of propagation to U (DPF=1/2 √ (3μs/μ_a)) [4], and g is the correction factor of the geometry. Based on the diffusion theory, the absorption coefficient (μ_a) can be calculated at any wavelength; this coefficient is assumed to be linearly independent for all the relevant molecules in the diffusing path, each having an extinction coefficient ϵ, leading to:

$$\epsilon C_n = \sum_{i=1}^{N} \varepsilon_{i,\lambda} C_i = \mu_a(\lambda) \quad (2)$$

According to Fig. 3, there are three different lengths of SD distance, which can be divided into three forward equations by the Beer Lambert Law. These three equations are named for the different length of SD: the first is "Equation a (Ea)" and the SD length equals 2U; the second is "Equation b (Eb)" and the SD length equals 4U; and the third is "Equation c (Ec)" and the SD length equals 6U.

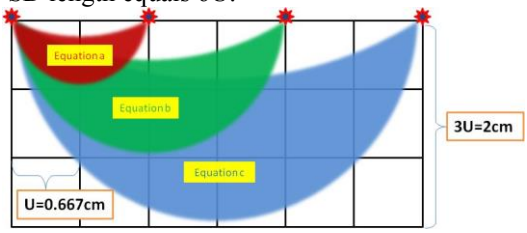

Figure 4. The cross sectional view schematic diagram of three forward equation.

For the Beer Lambert Law in (1), replacing some variables to simplify the equation with substitute variable can be shown as:

$$\begin{cases} O_{eq} = \frac{I_d}{I_i} \\ A_n = \exp(-\epsilon C_n U) \\ G_{eq} = \exp(-g) \end{cases} \quad (3)$$

O_{eq} is the ratio of light intensity of source and detector. A_n is the absorption factor of tissue for each unit grid. G_{eq} is the measurement geometry of the detector. After replacing the variables in (1), the Beer Lambert Law becomes simpler and can be shown as:

$$O_{eq} = \sum_m \{R_m \cdot \prod_n A_n^{P_n}\} \cdot G_{eq} \quad (4)$$

B. Variable Definition

Table 1 shows the different kinds of parameters with description, which include the physical parameters (absorption factor, intensity factor) and weighting coefficients (spatially, geometrically, algebra).

TABLE I. THE DESCRIPTION OF EACH VARIABLE

Variable name	Description
A(front index),(depth index)	Absorption factor of tissue for a unit grid
P(equation)(front index),(depth index),(forward term)	A differential path-length factor (DFP)
R(equation)(forward term)	the possibility of the light source and the receiver with diffusing path of different depth
E(equation)(front index),(forward term)	The information of the photons diffusion process
O(equation)(front index)	The light intensity ratio of the source and detector
G(equation)	The measurement geometry of the detector
D(equation)(inverse term),(angle)	Reconstructed information for each grid
F(equation)(inverse term)	Ratio factor of the different light source in the diffusion process passes through the grid
H(equation)(previous term)	Weighting coefficient of the convergence

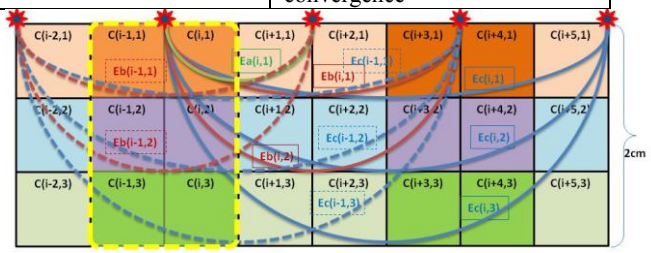

Figure 5. The cross sectional of the paths of each other three equations.

C. Formula Derivation

Fig. 5 shows the different light propagation paths according to different distances between sources and detectors. During the simulation, each source-detector pair is excited at different times in order to avoid crosstalk between two neighboring sources, so we ignore this phenomenon in this work. After simplifying the Beer Lambert Law equation by variable substitution, the three forward equations and inverse solutions can be written as the following:

- Top Layer

The forward equation for the Top layer is called "equation a", which crosses two units (U) in the front direction and consists of one forward term, and is represented by the solid green line (Ea (I, 1)) in Fig. 5. The Oai represents the ratio of output and input intensity from the equation "a" at the location I, and the forward equation formula is

$$\begin{cases} Ea_{i,1} = A_{i,1}^{Pa_{i,1,1}} A_{i+1,1}^{Pa_{i+1,1,1}} \\ Oa_i = Ra_1 Ea_{i,1} Ga \end{cases} \quad (5)$$

The term Ea is an intermediate variable. The inverse solution of equation "a" is

$$\begin{cases} \mathrm{Oa_i} = \mathrm{Ra_1 Ea_{i,1} Ga} \\ \mathrm{Ea_{i,1}}' = \frac{\mathrm{Ea_{i,1}}}{\mathrm{A_{i,1}}'^{\mathrm{Pa_{i,1,1}}}} \end{cases}$$

$$\Longrightarrow \mathrm{Oa_i} = \mathrm{Ra_1 A_{i,1}}'^{\mathrm{Pa_{i,1,1}}} \mathrm{Ea_{i,1}}' \mathrm{Ga}$$

$$\Longrightarrow \mathrm{Da_{1,angle}} = \mathrm{A_{i,1}}' = \sqrt[\mathrm{Pa_{i,1,1}}]{\frac{\frac{\mathrm{Oa_i}}{\mathrm{Ga}}}{\mathrm{Ra_1 Ea_{i,1}}'}} \quad (6)$$

$$\mathrm{Da} = \mathrm{Fa_1} \frac{\sum_{\theta=0}^{5} \mathrm{Da_{1,60*\theta}}}{6}$$

The formula of A(i,j) and Da(1,angle) have six values to represent the six different directions. Da(1,angle) is the value of reconstructed information. In each iteration process, the final value of Da has average the six values in different directions. Fa is a weighting coefficient.

The new value of Da which is obtained from (6) will substitute into (7), the convergence equation. The equation is related to four previous results and the weighting coefficient Ha. The iteration constantly operated to correspond with the convergence condition (|Ba(t)-Ba(t-1)|<0.0001). If the computation corresponds to convergence condition, the value is nearly stable.

$$\mathrm{Ba(t)} = \mathrm{Ha_1 Da} + \mathrm{Ha_2 Ba(t-1)} + \mathrm{Ha_3 Ba(t-2)} + \mathrm{Ha_4 Ba(t-3)} \quad (7)$$

- Middle Layer

The forward equation for Middle layer is called "equation b" which crosses four units (U) in the front direction and consists of two forward terms and is represented by the solid red line (Eb(i,1), Eb(i,2)) in Fig. 5. The Obi represents the ratio of output and input intensity from equation "b" at the location i, and the forward equation formula is:

$$\begin{cases} \mathrm{Eb_{i,1}} = \mathrm{A_{i,1}}^{\mathrm{Pb_{i,1,1}}} \mathrm{A_{i+1,1}}^{\mathrm{Pb_{i+1,1,1}}} \mathrm{A_{i+2,1}}^{\mathrm{Pb_{i+2,1,1}}} \mathrm{A_{i+3,1}}^{\mathrm{Pb_{i+3,1,1}}} \\ \mathrm{Eb_{i,2}} = \mathrm{A_{i,1}}^{\mathrm{Pb_{i,1,2}}} \mathrm{A_{i,2}}^{\mathrm{Pb_{i,2,2}}} \mathrm{A_{i+1,2}}^{\mathrm{Pb_{i+1,2,2}}} \mathrm{A_{i+2,2}}^{\mathrm{Pb_{i+2,2,2}}} \times \mathrm{A_{i+3,2}}^{\mathrm{Pb_{i+3,2,2}}} \mathrm{A_{i+3,1}}^{\mathrm{Pb_{i+3,1,2}}} \\ \mathrm{Ob_i} = \left(\mathrm{Rb_1 Eb_{i,1}} + \mathrm{Rb_2 Eb_{i,2}}\right)\mathrm{Gb} \end{cases} \quad (8)$$

The inverse solution of equation "b" is given as

$$\begin{cases} \mathrm{Ob_i} = \left(\mathrm{Rb_1 Eb_{i,1}} + \mathrm{Rb_2 Eb_{i,2}}\right)\mathrm{Gb} \\ \mathrm{Eb_{i,2}}' = \frac{\mathrm{Eb_{i,2}}}{\mathrm{A_{i,2}}'^{\mathrm{Pb_{i,2,2}}}} \end{cases}$$

$$\Longrightarrow \mathrm{Ob_i} = \left(\mathrm{Rb_1 Eb_{i,1}} + \mathrm{Rb_2 A_{i,2}}'^{\mathrm{Pb_{i,2,2}}} \mathrm{Eb_{i,2}}'\right)\mathrm{Gb} \quad (9)$$

$$\Longrightarrow \mathrm{Db_{1,angle}} = \mathrm{A_{i,2}}' = \sqrt[\mathrm{Pb_{i,2,2}}]{\frac{(\mathrm{Ob_i}/\mathrm{Gb}) - \mathrm{Rb_1 Eb_{i,1}}}{\mathrm{Rb_2 Eb_{i,2}}'}}$$

When calculating the inverse solution of the second term, the location i can be replaced by the location (i-1) because the forward equation at location (i-1) is similar to location i. Equation (9) can be rewritten as following:

$$\mathrm{Ob_{i-1}} = \left(\mathrm{Rb_1 Eb_{i-1,1}} + \mathrm{Rb_2 Eb_{i-1,2}}\right)\mathrm{Gb}$$

$$\mathrm{Eb_{i-1,2}}' = \frac{\mathrm{Eb_{i-1,2}}}{\mathrm{A_{i-1,2}}'^{\mathrm{Pb_{i-1,2,2}}} \mathrm{A_{i,2}}'^{\mathrm{Pb_{i,2,2}}}}$$

$$\Longrightarrow \mathrm{Ob_{i-1}} = (\mathrm{Rb_1 Eb_{i-1,1}} + \mathrm{Rb_2 A_{i-1,2}}'^{\mathrm{Pb_{i-1,2,2}}} \times \mathrm{A_{i,2}}'^{\mathrm{Pb_{i,2,2}}} \mathrm{Eb_{i-1,2}}')\mathrm{Gb}$$

$$\Longrightarrow \mathrm{Db_{2,angle}} = \mathrm{A_{i-1,2}}' = \sqrt[\left(\mathrm{Pb_{i-1,2,2}} + \mathrm{Pb_{i,2,2}}\right)]{\frac{(\mathrm{Ob_{i-1}}/\mathrm{Gb}) - \mathrm{Rb_1 Eb_{i-1,1}}}{\mathrm{Rb_2 Eb_{i-1,2}}'}} \quad (10)$$

The formula of A(i,j) has twelve values to represent six different directions for two inverse term formulas in (9) and (10). Db is the value of reconstruction information. In each iteration process, the final value of Db has the average six Db(1,angle) and Db(2,angle) in (11). Fb is a weighting coefficient which is determined by the Monte-Carlo-forward-model to calculate the crossing probability to the corresponding inverse term at A(i,j):

$$\mathrm{Db} = \mathrm{Fb_1} \frac{\sum_{\theta=0}^{5} \mathrm{Db_{1,60*\theta}}}{6} + \mathrm{Fb_2} \frac{\sum_{\theta=0}^{2} \mathrm{Db_{2,60*\theta}}}{3} \quad (11)$$

Equation (12), the convergence equation, is related to the four previous results. The iteration constantly operates to correspond with the convergence condition (|Bb(t)-Bb(t-1)|<0.0001). If the computation corresponds to the convergence condition, the value is nearly stable.

$$\mathrm{Bb(t)} = \mathrm{Hb_1 Db} + \mathrm{Hb_2 Bb(t-1)} + \mathrm{Hb_3 Bb(t-2)} + \mathrm{Hb_4 Bb(t-3)} \quad (12)$$

- Bottom Layer

The forward equation for Bottom layer is called "equation c" which crosses six units (6U) in the front direction and consists of three forward terms and is represented by the solid blue line (Ec(i,1), Ec(i,2), Ec(i,3)) in Fig. 5. The Oci represents the ratio of output and input intensity from equation "c" at location I, and the forward equation formula is.

$$\begin{cases} \mathbf{Ec_{i,1}} = \mathrm{A_{i,1}}^{\mathrm{Pc_{i,1,1}}} \mathrm{A_{i+1,1}}^{\mathrm{Pc_{i+1,1,1}}} \mathrm{A_{i+2,1}}^{\mathrm{Pc_{i+2,1,1}}} \times \mathrm{A_{i+3,1}}^{\mathrm{Pc_{i+3,1,1}}} \mathrm{A_{i+4,1}}^{\mathrm{Pc_{i+4,1,1}}} \mathrm{A_{i+5,1}}^{\mathrm{Pc_{i+5,1,1}}} \\ \mathbf{Ec_{i,2}} = \mathrm{A_{i,1}}^{\mathrm{Pc_{i,1,2}}} \mathrm{A_{i,2}}^{\mathrm{Pc_{i,2,2}}} \mathrm{A_{i+1,2}}^{\mathrm{Pc_{i+1,2,2}}} \mathrm{A_{i+2,2}}^{\mathrm{Pc_{i+2,2,2}}} \times \mathrm{A_{i+3,2}}^{\mathrm{Pc_{i+3,2,2}}} \cdots \mathrm{A_{i+5,2}}^{\mathrm{Pc_{i+5,2,2}}} \mathrm{A_{i+5,1}}^{\mathrm{Pc_{i+5,1,2}}} \\ \mathbf{Ec_{i,3}} = \mathrm{A_{i,1}}^{\mathrm{Pc_{i,1,2}}} \mathrm{A_{i,2}}^{\mathrm{Pc_{i,2,2}}} \mathrm{A_{i+1,2}}^{\mathrm{Pc_{i+1,2,2}}} \mathrm{A_{i+2,2}}^{\mathrm{Pc_{i+2,2,2}}} \times \mathrm{A_{\iota+5,3}}^{\Pi\chi_{\iota+5,3,3}} \mathrm{A_{\iota+5,2}}^{\Pi\chi_{\iota+5,2,3}} \mathrm{A_{\iota+5,1}}^{\Pi\chi_{\iota+5,1,3}} \\ \mathrm{Ob_i} = \left(\mathrm{Rc_1 Ec_{i,1}} + \mathrm{Rc_2 Ec_{i,2}} + \mathrm{Rc_3 Ec_{i,3}}\right)\mathrm{Gc} \end{cases} \quad (13)$$

The Inverse solution of equation "c" is given as

$$\begin{cases} \mathrm{Oc_i} = \left(\mathrm{Rc_1 Ec_{i,1}} + \mathrm{Rc_2 Ec_{i,2}} + \mathrm{Rc_3 Ec_{i,3}}\right)\mathrm{Gc} \\ \mathrm{Ec_{i,3}}' = \frac{\mathrm{Ec_{i,3}}}{\mathrm{A_{i,3}}'^{\mathrm{Pc_{i,3,3}}}} \end{cases}$$

$$\mathrm{Oc_i} = \left(\mathrm{Rc_1 Ec_{i,1}} + \mathrm{Rc_2 Ec_{i,2}} + \mathrm{Rc_3 A_{i,3}}'^{\mathrm{Pc_{i,3,3}}} \mathrm{Ec_{i,3}}'\right)\mathrm{Gc}$$

$$\mathrm{Dc_{1,angle}} = \mathrm{A_{i,3}}' = \sqrt[\Pi\chi_{\iota,3,3}]{\frac{(\mathbf{Oc_i}/\Gamma\chi) - \mathrm{P}\chi_1 \mathbf{Ec_{i,1}} - \mathrm{P}\chi_2 \mathbf{Ec_{i,2}}}{\mathrm{P}\chi_3 \mathbf{Ec_{i,3}}'}} \quad (14)$$

When calculating the inverse solution of second term, the location i can be replaced by the location (i-1) because the forward equation at location (i-1) is similar to the location i. Equation (14) can be rewritten as following:

$$\begin{cases} Oc_{i-1} = \left(\mathrm{Rc_1} Ec_{i-1,1} + \mathrm{Rc_2} Ec_{i-1,2} + \mathrm{Rc_3} Ec_{i-1,3}\right)\mathrm{Gc} \\ E_{i-1,3}' = \frac{Ec_{i-1,3}}{A_{i-1,3}'^{\mathrm{Pc_{i-1,3,3}}} A_{i,3}'^{\mathrm{Pc_{i,3,3}}}} \end{cases}$$

$$\Longrightarrow \mathrm{Oc_i}=\left(\mathrm{Rc_1Ec_{i,1}}+\mathrm{Rc_2Ec_{i,2}}+\mathrm{Rc_3{A_{i,3}}'^{Pc_{i,3,3}}Ec_{i,3}}'\right)\mathrm{Gc}$$

$$\Longrightarrow \mathrm{Dc_{1,angle}}=\mathrm{A_{i,3}}'$$

$$=\sqrt[\Pi\chi_{i,3,3}]{\frac{(\mathrm{Oc_i}/\Gamma\chi)-\mathrm{P\chi_1Ec_{i,1}}-\mathrm{P\chi_2Ec_{i,2}}}{\mathrm{P\chi_3Ec_{i,3}}'}} \quad (15)$$

$$\mathrm{Dc}=\mathrm{Fc_1}\frac{\sum_{\theta=0}^{5}\mathrm{Dc_{1,60*\theta}}}{6}+\mathrm{Fc_2}\frac{\sum_{\theta=0}^{5}\mathrm{Dc_{2,60*\theta}}}{6} \quad (16)$$

Equation (17), the convergence equation, is related to four previous results. The iteration constantly operates to correspond with the convergence condition (|Bc(t)-Bc(t-1)|<0.0001). If the computation corresponds to the convergence condition, the value is nearly stable.

$$\mathrm{Bc(t)}=\mathrm{Hc_1Dc}+\mathrm{Hc_2Bc(t-1)}+\mathrm{Hc_3Bc(t-2)}+\mathrm{Hc_4Bc(t-3)} \quad (17)$$

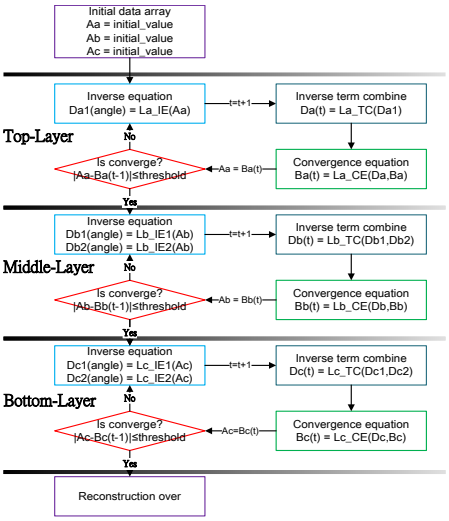

Figure 6. The image reconstruction process

D. Reconstruction Process

Fig. 6 is the reconstruction flow; the reconstruction order is layer by layer, from the top layer to the bottom layer. At first, when the initial condition is given, the reconstruction computes the inverse equation and inverse term. Then the reconstruction judges whether the convergence equation will correspond or not. Once the convergence condition corresponds, it will carry out the next layer reconstruction. After the layer completes the reconstruction, it will be considered as the known value to help the reconstruction of the next layer.

III. Simulation Results

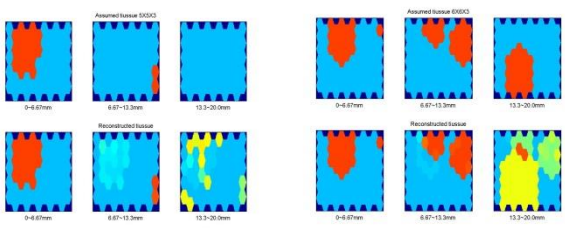

Figure 7. Simulation Results

In the simulation the wavelength is set at 730 nm. The absorption coefficient of the background is 0.12 cm^{-1}. The absorption coefficient of the abnormal area is 0.31 cm^{-1}, and the scattering coefficient is 15 cm^{-1}. The condition of the first iteration is set that the space is homogeneous in that the absorption coefficient of the background is constant. In the picture, the normal tissue is assumed to be light blue; the orange is the abnormal tissue. The upper three figures show the assumed tissue with different layers and the lower three figures represent the reconstructed image with different layers. According to the simulation results, the reconstruction algorithm can parse the two layers clearly. With the increase of the number of the layers, the cumulative error will be too large to reconstruct the third layer clearly, so its simulation result is not as good as the other layers. But it still has a reference value for the shallow foreign body diagnosis.

IV. Conclusions

The hexagonal structure provides more associated detection region in symmetries. The non-linear algorithm is developed by observing the phenomenon of light propagation from previous Monte Carlo based forward-model iteration techniques. In this paper, the proposed approach incorporates a multiple-input multiple-output (MIMO) based data extraction algorithm for a hexagonal source and detector array structure, to reconstruct the images of three layers. We applied a non-linear iterative approach to make convergence easier. The simulation results are nearly identical to the original images. It can parse the two layers clearly. Although the operation of the third layer is not as good as the other layers. The algorithm not only enhances the reconstruction accuracy by increasing the scanning amount of each grid but also achieves multiple layers.

Acknowledgment

This work was supported in part by the Ministry of Science and Technology of Taiwan, R.O.C., under grant NSC102-2220-E-009-033 and 101-2221-E-009-169-MY2.

References

[1] JongKwan Choi; MinGyu Choi; Hyeon-Min Bae, "An efficient data extraction method for high-temporal-and-spatial-resolution near infrared spectroscopy (NIRS) systems," Circuits and Systems (ISCAS), 2012 IEEE International Symposium on , vol., no., pp.560,563, 20-23 May 2012.

[2] D. A. Boas, D. H. Brooks, E. L. Miller, C. A. DiMarzio, M. Kilmer, R. J. Gaudette, and Q. Zhang, "Imaging the body with diffuse optical tomography," Signal Process., vol. 21, pp. 57–75, Nov. 2002.

[3] S. Bunce, M. Izzetoglu, K. Izzetoglu, B. Onaral, and K. Pourrezaei,"Functional near infrared spectroscopy: An emerging neuroimaging modality,"IEEE Eng. Med. Biol. Mag, vol. 25, no. 4, pp. 54-62, 2006.

[4] Boas D A, Gaudette T, Strangman G, Cheng X, Marota J A and Mandeville J B, "The accuracy of near infrared spectroscopy and imaging during focal changes in cerebral hemodynamics," Neuroimage 13 76–90, 2001